Materialia 000 (2018) 1–6

Contents lists available at ScienceDirect

Materialia

journal homepage: www.elsevier.com/locate/mtla

Full Length Article

High permittivity behavior and microstructure in a two-phase barium-silicon titanate

Dennis S. Tucker[a,*], Curtis W. Hill[a], Xuyang Zhou[b], Gregory Thompson[b], Baisheng Ma[c], Zhongyang Chang[c]

[a] EM32, Marshall Space Flight Center, Huntsville, AL 35812, USA
[b] Department of Metallurgical and Materials Engineering, Tuscaloosa, Al 35487-0202, USA
[c] Materials Research and Education Center, Auburn University, Auburn, AL 36849-5341, USA

ARTICLE INFO

Keywords:
Permittivity
Barium titanate
Polaron
Faulting

ABSTRACT

Barium titanate (140 nm) was coated with silicon dioxide using atomic layer deposition after which the powders were sintered at 1050 °C for 5 min at 50 MPa using a direct current sintering furnace. Dielectric measurements showed large permittivity (up to 4×10^5) with X-ray and electron diffraction confirming a cubic titanate and tetragonal silicate-based mixture. Transmission electron microscopy revealed planar faults within the tetragonal phase where such defects could assist in the charge storage along with grain boundaries. Polaron relaxation was also observed in this material.

Barium titanate ($BaTiO_3$), also abbreviated as BTO, is known for its high dielectric constant ($\sim10^3$) in the range from 100 Hz to 1 MHz leading to applications as high performance capacitors, multilayer capacitors, energy storage devices, and thermistors [1–7]. To further improve the properties of BTO, rare earth oxides have been studied as additives. These rare earth additions are used to control the Curie point temperature as well as improve electrical properties by regulating the grain size and microstructure [7–13]. In yet another microstructural approach, BTO particles have been coated with a thin oxide layer which leads to a core/shell structure which is believed to inhibit grain growth which can also assist in achieving similar property improvements [14].

A common approach to coating BTO is to use a sol-gel process. In one study, BTO was doped with 0.5 mol% Nb_2O_5, was sol-gel coated with silicon dioxide and subsequently sintered via uniaxial hot pressing [14]. Cernea et al. [14] found an increase in the dielectric constant and a decrease in the dielectric loss for the sample coated versus the uncoated sample. In another study, Chung et al. [15] used a modified sol-gel process to obtain a 5 nm coating of silica on 500 nm diameter BTO particles. Post-coating, they were spark plasma sintering (SPS) to densify the sample and similarly observed a dielectric constant up to 2×10^5 at 10^4 Hz with a very low dielectric loss of ~5% at 10^4 Hz. A space charge relaxation at the grain boundaries was proposed as the charge storage mechanism.

One of the consequences of silica coatings with BTO is the potential deleterious reactions of the species with each other forming either $BaTiSiO_5$ or $Ba_2TiSi_2O_8$ when exposed to high temperatures [16–18]. Though not all silica coated-BTO studies have provided a detailed characterization of phase and microstructure content, in those that have, the formation of these phases is apparent. The dielectric constant of these two new compounds is lower than that of BTO [16]. Thus, it is difficult to understand the origins of the high dielectric constant observed in, for example, SPS processed SiO_2 coated BTO. In this paper, we undertake a study on the microstructure of SPS processed atomic layer deposited (ALD) SiO_2 on BTO to help elucidate the mechanisms responsible for the observed improvements in the dielectric properties. We are also interested in whether or not the ALD coating technique is appropriate for this system.

The silica coatings were applied to the BTO powders using atomic layer deposition (ALD). ALD provides a sequential, self-limiting, layer-by-layer deposition mode over our BTO powders. [19] Unlike the prior means of silica coating, ALD offers several advantages. It is reported to produce very conformal and ultra-thin films with excellent composition and thickness control at the angstrom level [20,21]. The processing advantage of ALD coatings for this study will enable potential control of the defect structure of the material and its relationship to the charge storage mechanisms.

The BTO powders, with a mean 140 nm diameter, were purchased from the Sakai Chemical Company (Japan) with the silica ALD coating performed by Vapor Pulse Inc. (Raleigh, NC, USA). The precursors used were tris(dimethylamino)silane and ozone. The deposition rate was 0.6 Å/cycle and 100 cycles were used to deposit the silica coating. Post-coating, the powders were loaded into a 20 mm graphite die lined with

* Corresponding author.
E-mail address: dr.dennis.tucker@nasa.gov (D.S. Tucker).

https://doi.org/10.1016/j.mtla.2018.07.015
Received 4 April 2018; Received in revised form 9 July 2018; Accepted 26 July 2018
Available online xxx
2589-1529/

grafoil film and sintered in a direct current sintering furnace at 1050 °C under 50 MPa applied pressure for 5 min with the sintering performed at $\sim 2 \times 10^{-3}$ Torr. Samples were heated at a rate of 100 °C/min to 950 °C and held for two minutes and then heated at a rate of 50 °C/min to 1050 °C to avoid overshooting the final temperature. In order to avoid fracture of the samples upon cool-down, once the 5 min soak at 1050 °C was completed, the current was turned off and the pressure removed yielding a~ 2 °C/min cooling rate. A crystallographic transformation from cubic-to-tetragonal occurs at 130 °C for BTO, with a rather large unit cell change which can lead to cracking [22]. It was found that if the cooling rate was too high and some residual pressure remained, the samples fractured. After removal of the sample from the graphite die, the grafoil was removed via polishing with SiC abrasive paper. It was observed that the sintered samples had a dark blue color indicating reduction. The samples were then washed in an acetone bath in an ultrasonic cleaner and then dried in an oven at 120 °C for 20 min. Gold was then sputtered on both sides of the sample which served as electrodes for the dielectric constant and dielectric loss characterization. The dielectric tests were carried out in an Agilent 4294A impedance analyzer from 100 Hz to 1 MHz using a Cp~D function with the dielectric constant calculated based on the measured results using the parallel plate model. The AC signal used in the measurements was 0.5 V. For the temperature dependent dielectric properties, the sample was heated to 140 °C with the temperature lowed at intervals of 10 °C. At each temperature, the sample was held for ten minutes to ensure thermal equilibrium.

The phase and microstructure of the samples were characterized using X-ray Diffraction (XRD) and (Scanning) Transmission Electron Microscopy ((S)TEM). The XRD was performed in a Phillips Diffractometer using Cu Kα ($\lambda_{Cu} = 0.1541$ nm) as the source. The phases from the XRD scans were further confirmed by electron diffraction in an FEI Tecnai F20 (S)TEM. The TEM sample was prepared by a focus ion beam (FIB) lift-out and annular milling procedure in either a TESCAN LYRA FIB-Field Emission Scanning Electron Microscope (SEM) or an FEI Quanta 3D dual beam FIB-SEM. The grain morphology and sizes were captured by bright field TEM and STEM-High Angle Annular Dark Field (HAADF) images, where the latter imaging mode generates contrast based on the atomic number, Z, of the elements in the phase, with higher Z elements being brighter. High resolution TEM (HRTEM) lattice fringe images of defects and interfaces between the phases in the microstructure were also captured at a defocus value of zero. X-ray Energy Dispersive Spectroscopy (EDS) maps were performed to qualitatively measure the composition of the sample and any potential chemical partitioning.

From the data shown in Fig. 1, one can find that the dielectric response originates from a relaxation process and a low-frequency process. The former results in a giant value (~10^5) of the permittivity in the low frequency range and a high loss at certain frequency (relaxation frequency, 10^4 to 10^6 Hz in the temperature range studied). The relaxation frequency increases with increasing temperature. The giant permittivity also increases with increasing temperature. For example, the permittivity at 100 Hz is about 2.2×10^5 and 3.9×10^5 at −50 and 140 °C, respectively. It can be noted in Fig. 1b that the loss is high. As can be seen from Fig. 2, not all particles were coated. There is also aggregation of particles. Both of these phenomena could lead to regions of the sintered material not having silica interfaces between the BTO particles. This could lead to high loss as noted in this study. For further discussion see supplemental material.

Fig. 2 is TEM image of the ALD coated particles, revealing the core-shell structure prior to sintering. The silica coating was found to vary from near 0 to 15 nm over the powders. Regardless of this thickness variation, the BTO powders have been coated creating a silica barrier between the powders upon sintering. Fig. 3(a) is the XRD scan for the sample post-sintering. The pattern clearly reveals a two phase mixture with the phases identified as the BTO *Pm3m* cubic phase with a lattice constant 0.402 nm and $Ba_2TiSi_2O_8$ *P4bm* tetragonal phase with lattice constants of a = b = 0.864 nm and c = 0.517 nm. Note the simulation pattern of each phase at the bottom of the figure. In Fig. 3(b)–(d), the

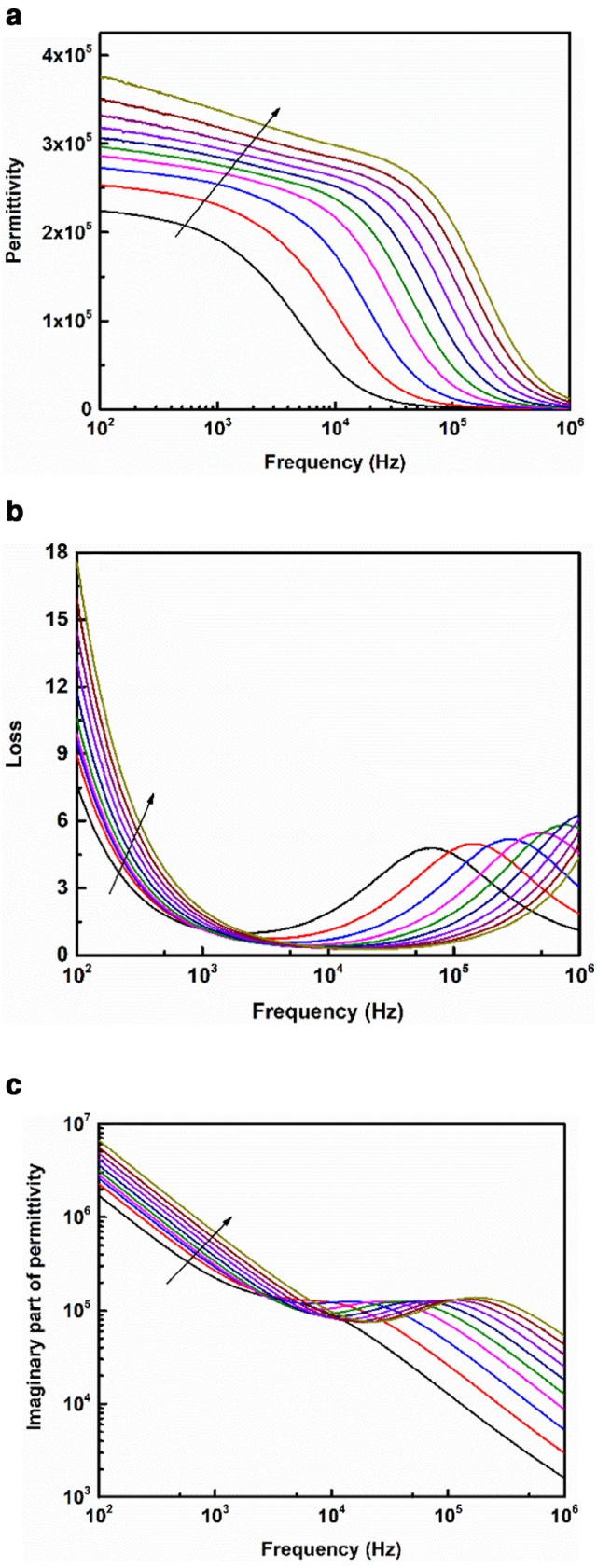

Fig. 1. Real part of permittivity (a), loss tangent (b) and imaginary part of permittivity **(c)** versus frequency for the sample at different temperatures. In the figure, each curve means the results at one temperature. The arrows are used to indicate the direction of temperature increase from −50 °C to 130 °C with an interval of 20 °C.